Measurement 231 (2024) 114565

Contents lists available at ScienceDirect

Measurement

journal homepage: www.elsevier.com/locate/measurement

Augmented-Resolution Digital image correlation algorithm for vibration measurements

Paolo Neri

University of Pisa. Department of Civil and Industrial Engineering, Mechanical Division. Largo L. Lazzarino 1, 56122 Pisa, Italy

ARTICLE INFO

Keywords:
Digital Image Correlation
Sub-pixel accuracy
Image resizing
Full-field vibration measurements
Augmented Resolution

ABSTRACT

Digital Image Correlation (DIC) is a widespread technique, and many different implementations were developed in the literature to optimize the algorithm performance. In this paper, a new DIC algorithm is optimized for vibration measurements, where the displacement amplitude drastically decreases with the increase in frequency. Even if high-resolution cameras are used, it is mandatory to use a DIC algorithm with reliable sub-pixel performance. DIC algorithms are generally optimized for large complex displacement fields, and they solve the sub-pixel problem by fitting correlation data through a second-order polynomial function. An innovative solution is proposed to push the sub-pixel accuracy and increase the signal-to-noise ratio of the measurement, by exploiting image resizing to achieve virtual higher resolutions and by adopting a quartic polynomial function to interpolate the displacement map with an increased number of interpolation points. The proposed algorithm is validated through synthetic and experimental data and compared to literature DIC algorithms.

1. Introduction

Vibration measurement is a crucial issue in the industry, from component characterization [1,2] and qualification to health monitoring setups [3,4]. Since high-frequency vibrations are generally characterized by complex deformed shapes, full-field measurement techniques are gaining increasing interest. In this scenario, Digital Image Correlation (DIC) surely represents a promising option for obtaining high-sensitivity full-field displacement maps in 2D or 3D [5–12]. Several different measurement approaches are available in the literature, based on different optical devices which range from high-speed low-resolution cameras [13–15] to low-speed high-resolution cameras exploiting down-sampling approaches [16,17]. Despite the acquisition strategy, the crucial step of DIC vibration measurement is represented by image elaboration to retrieve displacement information basing on speckle pattern identification. Two main families of DIC methods can be found in literature: local methods [18,19], where each measurement point is processed independently, and global methods [20,21], where the whole point grid is processed altogether. The first approach is faster and does not require any constraint about the measurement point grid, nor exploits any hypothesis about the displacement field. Additionally, sub-pixel accuracy can be achieved by interpolating the correlation map close to the maximum through a quadratic polynomial form. The main drawback is that the point-by-point displacement continuity is not guaranteed, since the measurement results are independently obtained for each measurement point, which can result in high noise in the spatial domain. On the other hand, global methods are generally based on a finite-element-like approach, so that the measurement points are organized in elements and simultaneously processed to guarantee global compatible displacements through optimization and smoothing approaches. The drawback is a much longer computational time, and compatibility constraints and smoothing are applied to the displacement maps, with the risk of artifacts in the measurements. Additionally, cracks or local damages can generate a discontinuity in the displacement map, but this information can be lost when global methods are used. Finally, some hybrid methods can be found in the literature [22–24], which exploit local methods to obtain a first guess of the displacement map which is then refined through a global approach. Even if the global DIC approach looks promising, its computational cost can be a burden and the need for constraints on the displacement maps can result in loss of generalization. Furthermore, since hybrid methods are still based on the results of local methods, improving the sensitivity of local methods can also be beneficial in the framework of a global method implementation. The need for improved sensitivity and a lower noise level in DIC elaboration is even more urgent in the case of vibration measurements. High-frequency response is characterized by complex shapes and really small displacements, which can easily drop in the range of 0.01 pxl. For these reasons, this paper is focused on the development of an

E-mail address: paolo.neri@unipi.it.

https://doi.org/10.1016/j.measurement.2024.114565
Received 10 July 2023; Received in revised form 20 March 2024; Accepted 22 March 2024
Available online 26 March 2024

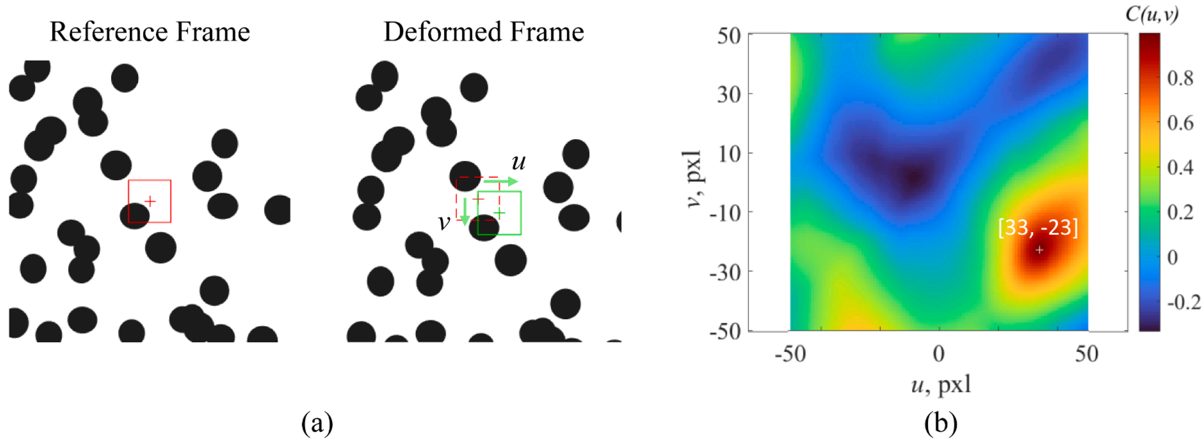

Fig. 1. Main working principle of DIC algorithms: (a) subsets definition and (b) correlation coefficient.

improved local method that can further enhance the sub-pixel sensitivity of the DIC technique, still allowing for the detection of local damage and displacement discontinuity. In particular, different approaches will be investigated to achieve this goal. Firstly, image resolution will be enhanced by exploiting pixel interpolation schemes to obtain augmented-resolution images. Secondly, the correlation interpolation scheme will be modified by exploiting a quartic polynomial function (instead of the conventional quadratic form) and by increasing the number of interpolation points around the maximum. A new DIC algorithm is then defined, named the Augmented Resolution Digital Image Correlation (AR-DIC) algorithm, whose parameters can be set to change the resolution magnification value, the interpolating polynomial function and the number of interpolation points. The effects of each parameter and their combinations are analyzed in the paper. The proposed algorithm was firstly validated through a simulated test: a synthetic image set with a known sinusoidal displacement with sub-pixel amplitude was numerically produced and processed through DIC. The results obtained with the AR-DIC algorithm were compared with well-known literature algorithms based on local methods, i.e. Digital Image Correlation and Tracking (DICT) algorithm [19] and the Open source 2D digital image correlation MATLAB program (Ncorr) algorithm [18]. The performance comparison among the tested algorithms was achieved by computing the signal-to-noise ratio (SNR) obtained in the measurement. The analysis of synthetic images allows to assess the performances of different algorithms under known and controlled conditions, both in terms of displacement amplitudes and noise. Nonetheless, the actual algorithm validation needs to be performed on real images. Thus, all the algorithms were compared through experimental data measured on a vibrating cantilever plate. The same image sequence was elaborated with the different algorithms and the results were compared both in time and spatial domain in terms of SNR values.

2. Augmented resolution DIC algorithm

All the local DIC algorithms available in the literature exploit 2D correlation to recognize image subsets along the deformed frames to assess displacement. The main algorithm architecture consists of parameters setup, measurement grid definition, raw displacement measurement at the pixel level and displacement refinement at the sub-pixel level. Fig. 1 shows the main idea for a single measurement point: a subset is defined around the measurement pixel (Fig. 1(a)) and its location over frames is searched by exploiting correlation (Fig. 1(b)). The correlation coefficient can be expressed in the form:

$$C(u,v) = \frac{\sum_{i,j}(r(i,j)-\overline{r})(d(i-u,j-v)-\overline{d})}{\sqrt{\sum_{i,j}(r(i,j)-\overline{r})^2\sum_{i,j}(d(i-u,j-v)-\overline{d})^2}} \tag{1}$$

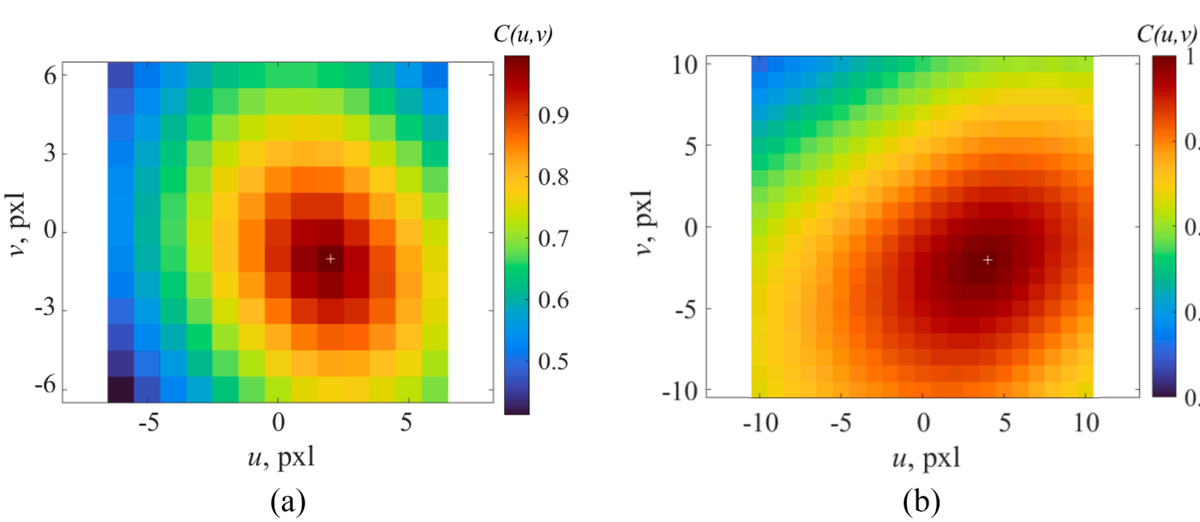

Fig. 2. Correlation map obtained for a synthetic displacement: (a) original images and (b) resized image with bicubic interpolation.

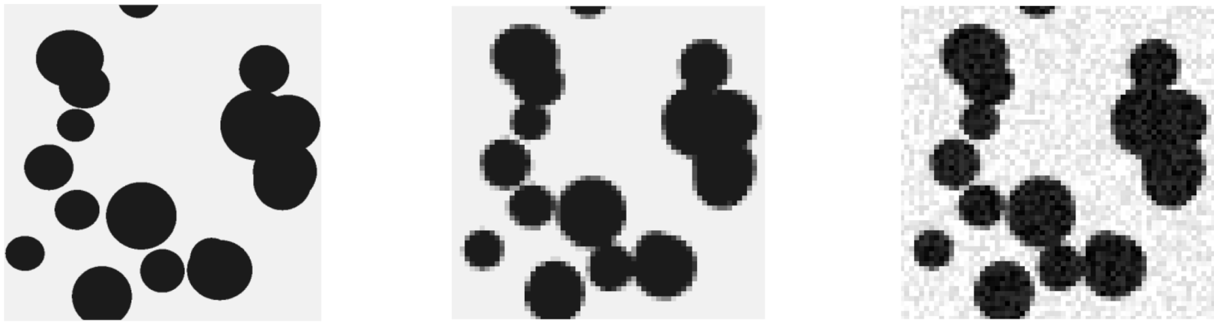

Fig. 3. Synthetic image generation: (a) vectorial image, (b) printed image with finite resolution and (c) printed image with added noise.

In Eq.1, the indexes i, j refer to the image pixel indexes, while u, v refer to the tentative displacement along vertical and horizontal directions, respectively. The computation is to be performed between the subset in the reference image, i.e. r, and the subset in the deformed image, i.e. d. For normalization purposes, $\overline{r}$ and $\overline{d}$ represent the mean value of the reference and deformed subsets, respectively. Eq. (1) allows to explore a given number of pixels around the measurement point, and to compute the correlation between subsets if the displacement u, v is applied. Thus, a map of correlation values can be defined in the investigated region, and its maximum value corresponds to the actual displacement between images. An example of a correlation map is reported in Fig. 1(b) corresponding to the displacement of Fig. 1(a). As can be noted, the maximum correlation coefficient is found for a displacement $[u, v] = [33, -23]$ pxl (displacement value was drastically emphasized for representation purposes). It is worth noting that, since the correlation coefficient must be computed in the pixels domain, u and v in Eq. (1) can only have integer values. Subsequently, the sub-pixel displacement can be refined by fitting the correlation coefficient maps around the integer maximum value with different techniques. The same overall scheme will be followed in this paper, but two different strategies will be proposed to improve the DIC sensitivity.

2.1. Polynomial interpolation

Generally, sub-pixel accuracy is achieved by fitting the correlation map with different analytical shapes, and by performing least square fitting or non-linear optimization. The most commonly adopted fitting function is a second-order complete polynomial in the form [19,25–28]:

$$\widetilde{C_2}(x, y) = p_1x^2 + p_2xy + p_3y^2 + p_4x + p_5y + p_6 \tag{2}$$

where $\widetilde{C_2}(x,y)$ is the fitted value of the correlation coefficient at coordinates x, y (which can be non-integer real numbers) and the parameters p_i are to be determined through the fitting procedure. Starting from the maximum shown in Fig. 1(b), a surrounding region of width $n_p = 1$ pxl is selected, i.e. the eight pixels surrounding the integer value are considered, for a complete grid of 3×3 points. A pseudo-inverse algorithm can be adopted to compute the polynomial parameters of Eq. (2) with a least square approach [29]. Finally, it is possible to analytically find the maximum of the second-order polynomial. Two options were investigated in this paper to improve this fitting procedure: the first one is to enlarge the fitting region by changing n_p, i.e. the number of points of the correlation map which are considered for the fit. The second option is to change the fitting function, e.g. by increasing the order of the polynomial p_o. In particular, in this paper a fourth-order polynomial was considered ($p_o = 4$):

$$\begin{aligned}\widetilde{C_4}(x, y) = {} & p_1x^4 + p_2x^3y + p_3x^3 + p_4x^2y^2 + p_5x^2y + p_6x^2 + p_7xy^3 + p_8xy^2 \\ & + p_9xy + p_{10}x + p_{11}y^4 + p_{12}y^3 + p_{13}y^2 + p_{14}y + p_{15}\end{aligned} \tag{3}$$

While the second-order polynomial allows for an analytical solution of the maximum location, the fourth-order polynomial requires a numerical detection of the maximum, which can be obtained through a Newton-Raphson approach [30]. It is worth noting that the initial guess in this optimization problem is reliable since the maximum of the displacement map can be easily detected at the pixel level. The optimization is only needed to refine the maximum search at the sub-pixel scale, thus there is no risk of detecting a local maximum instead of a global maximum. For this reason, the optimization algorithm itself is not crucial, and different algorithms can mainly impact the computational performance rather than the result accuracy.

Table 1
Parameter combinations in the investigated cases for the AR-DIC algorithm.

Case N.	r_f	p_o	n_p
AR-DIC1	2	Quadratic	1
AR-DIC2	2	Quartic	1
AR-DIC3	2	Quartic	2

2.2. Image resizing

As clear from Eq. (1), the correlation map is mandatorily computed with the pixel resolution, since u and v must be integer values (hence the need for polynomial interpolation to achieve sub-pixel accuracy, as stated in Section 2.1). Nevertheless, it is possible to simulate non-integer shifts of u and v in Eq. (1) by numerically resizing the image frames. In this way, the displacement map can be directly computed with a sub-pixel resolution. The case of a resizing factor of $r_f = 2$ can be considered as an example. If the subsets are resized to double the original number of pixels, the new coordinates $u' = 2u$ and $v' = 2v$ must be considered to construct the correlation map. Now, an integer shift of 1 pxl along u' is equivalent to 0.5 pxl in the original image. This allows to refine the definition of the correlation map to the wanted extent, since the resizing procedure can be performed with an arbitrary r_f. Additionally, there are several different resizing algorithms available, which interpolate the image data with different functions. In particular, in this paper the Matlab function *imresize* with the bicubic interpolation will be considered. Fig. 2 shows an example of a correlation map obtained for a given synthetic displacement by processing the original images (Fig. 2(a)) and the resized images (Fig. 2(b)) by using the bicubic interpolation. The plots in Fig. 2(a) and (b) are referred to the same image region, but Fig. 2(b) shows twice the pixels because the resizing factor $r_f = 2$ was used. It can be noted that the correlation map gains more resolution and a smoother distribution, opening to the possibility of obtaining higher sub-pixel accuracy.

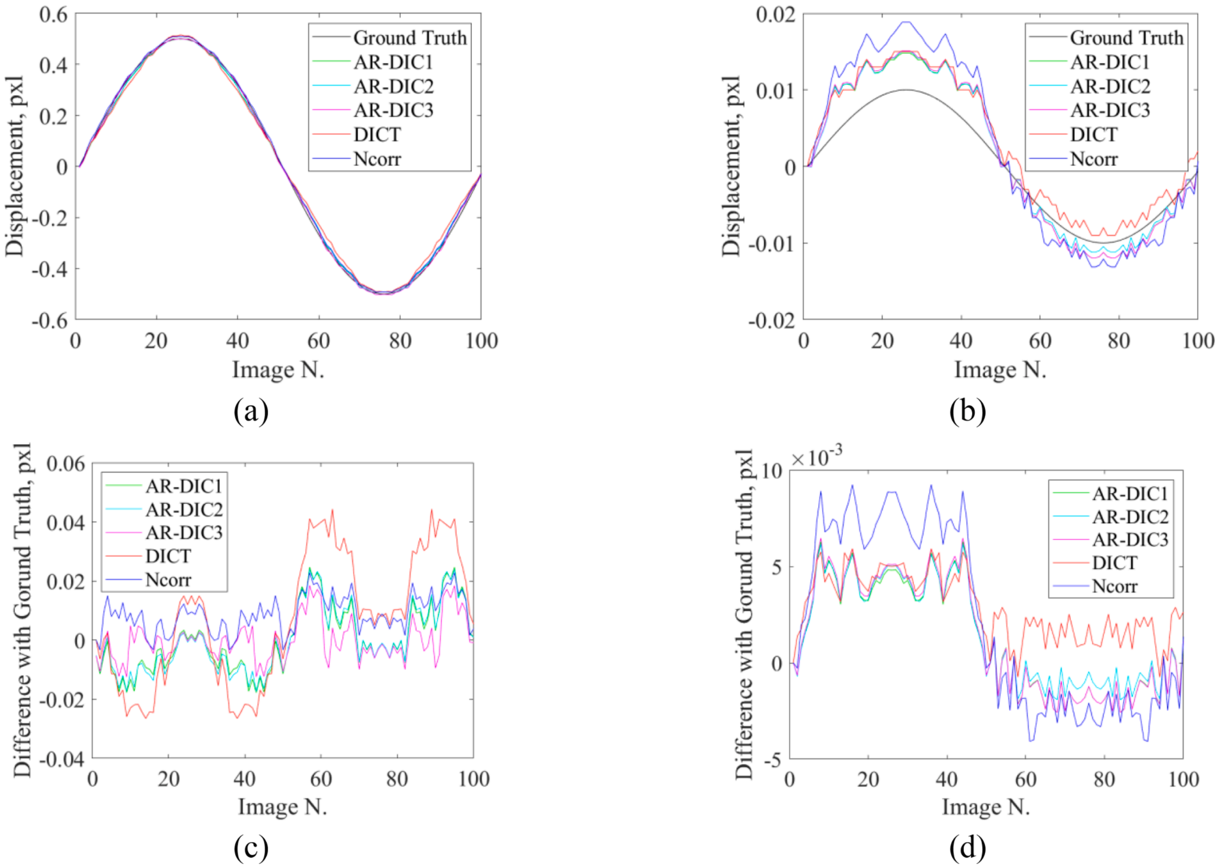

Fig. 4. Synthetic data without noise: displacements assessed by the algorithms for (a) 0.5 pxl amplitude and (b) 0.01 pxl amplitude; differences with Ground Truth for (c) 0.5 pxl amplitude and (d) 0.01 pxl amplitude.

3. Performance validation on synthetic data

3.1. Synthetic dataset generation

To assess the performance of different algorithms and different elaboration parameters, a synthetic image set was prepared to compare the algorithms with a controlled dataset, both in terms of displacement values and noise level. Since the paper aims to investigate sub-pixel accuracy, the speckled images were generated by analytically plotting a series of black ellipses with random centers and random principal axes lengths on a white background. In this way, an arbitrarily small displacement can be applied to all the speckle centers to simulate a rigid motion in the image plane. In particular, an adimensional image size of 1×1 was defined, and the principal axes of the elliptical speckles were set with the adimensional mean value of 0.05 and a standard deviation of 0.01. Then, the plot was converted into an image, so that the actual pixel values depend on the conversion resolution, simulating the acquisition by a finite-resolution sensor. The image was then printed as a frame, thus converting from a vector plot to a discretized image, resulting in an average speckle size of about 10 pxl and a standard deviation of about 2 pxl. By properly scaling the analytical displacement with respect to the synthetic image resolution, it is possible to obtain a controlled displacement with an arbitrary sub-pixel resolution. In particular, a sinusoidal displacement was considered in this paper, since the algorithm is intended for vibration measurements. An arbitrary number of periods and measurement instants can be defined, and the harmonic amplitude can be adjusted to set the sensitivity of different algorithms to small displacements. Additionally, it is possible to add random noise with arbitrary amplitude to the synthetic images to assess its effect on the final elaboration results. In the generated set, the random noise had a uniform distribution and an amplitude of 255/10, i.e. 1/10 the maximum value that is measurable on an 8-bit image. An example of synthetic image definition is reported in Fig. 3: Fig. 3(a) shows the adimensional analytical plot, Fig. 3(b) shows the discretized image frame and Fig. 3(c) shows the result with added noise.

3.2. Algorithm validation

The proposed algorithms were tested on synthetic data where a known sub-pixel displacement was applied along the x direction through a sinusoidal function with a given amplitude. The images were then processed through different algorithms: the proposed AR-DIC algorithm with different parameters and literature algorithms. In particular, two open-source algorithms were considered, whose implementation is available on Matlab Central and can be used for direct comparison: Digital Image Correlation and Tracking (DICT) [19] and the Open source 2D digital image correlation MATLAB program (Ncorr) [18]. The performance of each algorithm is assessed in terms of Signal-To-Noise Ratio (SNR). In particular, since the ground truth is known to be one period of a sinusoidal displacement, it was possible to compute the first harmonic of the measured displacement, which represents the signal (s), through conventional Fourier analysis. Then, the first harmonic was subtracted from the complete signal, to estimate the measurement noise (n). It was then possible to compute the SNR in Decibel as:

$$\mathrm{SNR} = 10\log_{10}\left(\mathrm{mean}(s^2)/\mathrm{mean}(n^2)\right) \tag{4}$$

Higher values of SNR correspond to a better performance of the algorithm. The literature algorithms were compared with the newly introduced one, by exploiting different combinations of the main parameters, i.e. image resizing factor (r_f), interpolating polynomial order (p_o) and the number of interpolation points (n_p), which are peculiar of the AR-

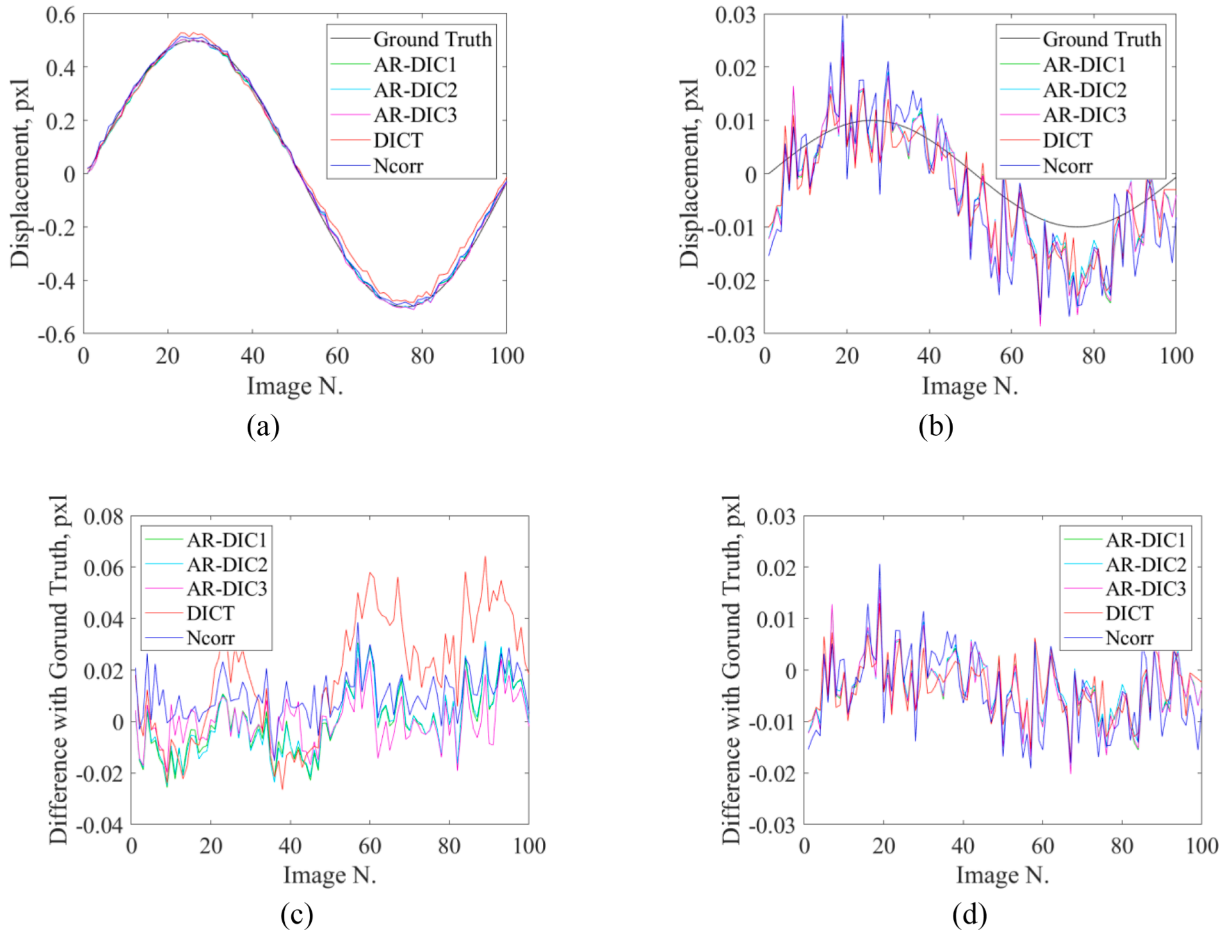

Fig. 5. Synthetic data with noise: displacements assessed by the algorithms for (a) 0.5 pxl amplitude and (b) 0.01 pxl amplitude; differences with Ground Truth for (c) 0.5 pxl amplitude and (d) 0.01 pxl amplitude.

Table 2
Comparison of different algorithms in terms of signal-to-noise ratio and computational time.

Algorithm	SNR, Db (0.5 pxl ampl.)		SNR, Db (0.1 pxl ampl.)		Computational Time, s
	Without Noise	With Noise	Without Noise	With Noise	
AR-DIC1	31.30	29.74	15.05	3.58	0.45
AR-DIC2	31.51	29.90	14.00	3.90	0.47
AR-DIC3	33.86	31.47	14.75	3.61	0.60
DICT	25.66	22.59	8.91	2.76	0.83
Ncorr	30.48	28.37	12.60	2.86	3.42

DIC algorithm. It is worth noting that different interpolation schemes are available for image resizing (e.g. bilinear or bicubic interpolation), but preliminary testing of different methods shows that the interpolation scheme does not significantly impact the DIC outcome in terms of SNR value, thus only bicubic interpolation was presented in the following. More precisely, three cases were considered to investigate the combination of different parameters, as reported in Table. 1. In all the cases, the resizing factor is set to 2, then for AR-DIC1 and AR-DIC2 $n_p = 1$ is set to interpolate a quadratic and a quartic polynomial respectively, while for AR-DIC3 a quartic polynomial is estimated by setting $n_p = 2$.

The same image set was then processed with all the described algorithms: all the DIC elaborations were performed with a subset size of 61 pxl (i.e. about six times the speckle dimension), and the center of the image was considered as the measurement point. The validation was firstly performed on a relatively high displacement amplitude of 0.5 pxl,

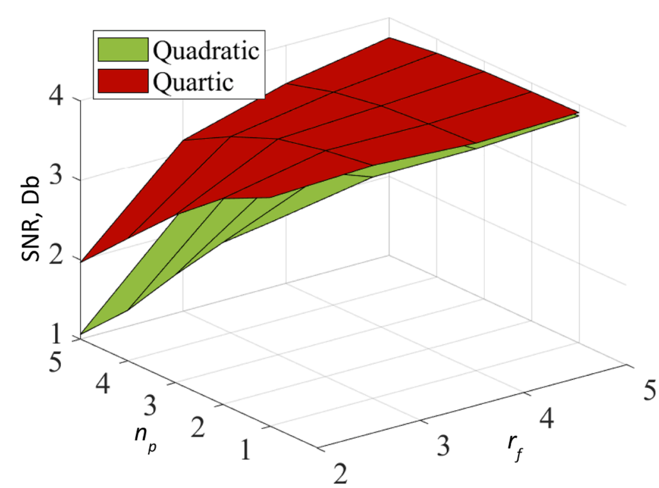

Fig. 6. Effect of different parameter values for AR-DIC, in the case of quadratic and quartic interpolation.

where high SNR values are expected. Then, the procedure was repeated to investigate extremely low displacement conditions, with an amplitude of 0.01 pxl (which is the sensitivity presented in [18,19] for the literature methods). The results obtained without added noise are reported in Fig. 4, comparing the theoretical displacement (black line) and the measured displacement. Fig. 4(a) shows the results corresponding to the 0.5 pxl amplitude, while Fig. 4(b) is referred to the 0.01 pxl

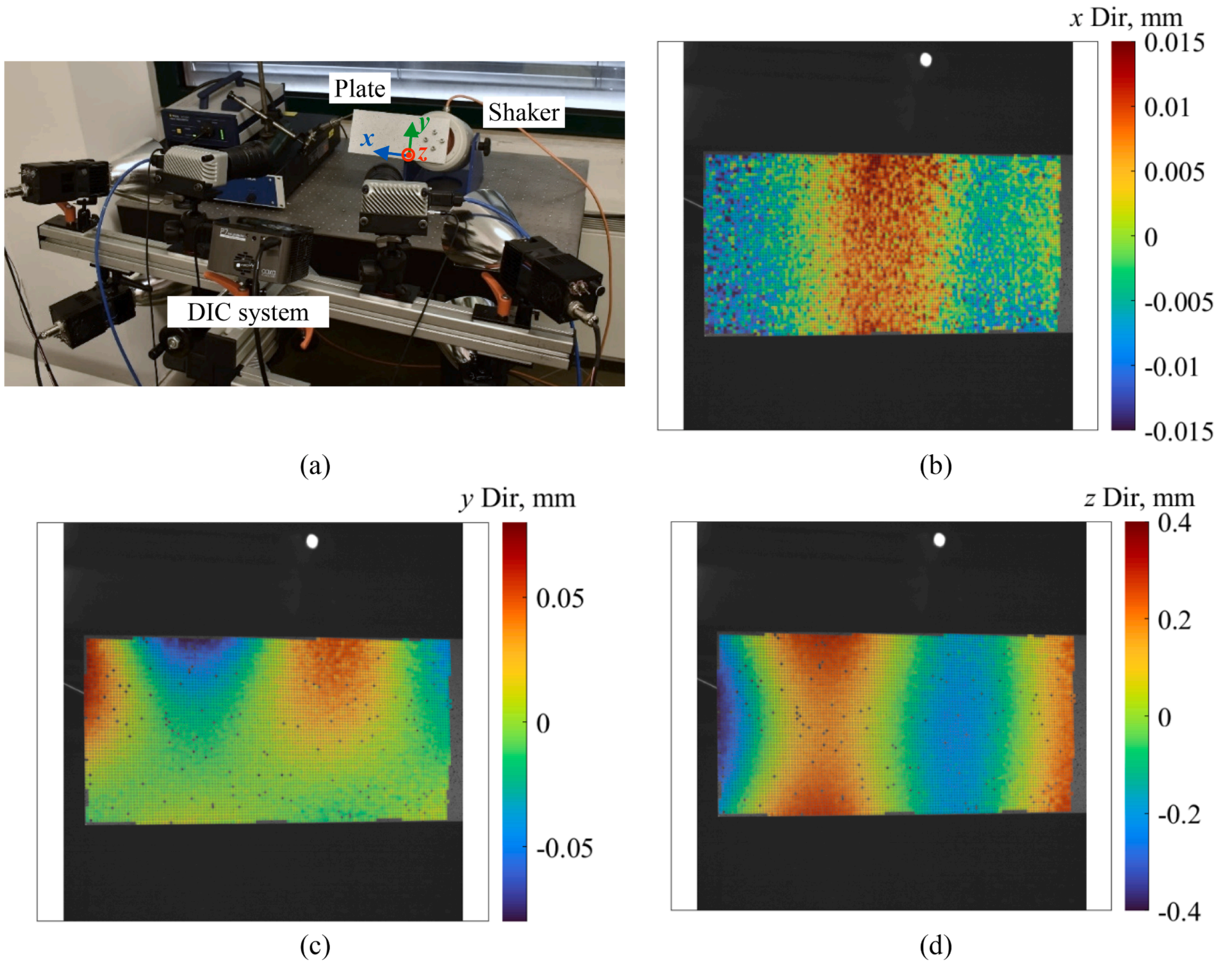

Fig. 7. Vibration test: (a) experimental setup and displacement map close to resonance at 591 Hz along (b) the x direction, (c) the y direction and (d) the z direction.

amplitude. Additionally, the difference between the ground truth displacement and the results of the different algorithms is reported in Fig. 4(c) and (d), for the cases of 0.5 pxl and 0.01 pxl amplitudes respectively. In particular, green, cyan and magenta lines in Fig. 4 show the performance of the AR-DIC algorithm for cases 1–3, respectively, while red and blue curves show the performance of the literature algorithms (DICT and Ncorr, respectively).

In the case of 0.5 pxl amplitude, the qualitative comparison of the curves in Fig. 4(a) does not highlight significant differences between the algorithms. Nevertheless, Fig. 4(b) shows that DICT has the greatest differences when compared with the ground truth. On the other hand, the differences between the AR-DIC algorithms and the Ncorr algorithm with ground truth are comparable in amplitude, but the Ncorr difference is always positive, meaning that the mean value of the displacement is erroneously detected. Considering Fig. 4(b), it is worth noting that, even if 0.01 pxl is provided as reference sensitivity for both DICT and Ncorr [18,19], this low value pushes all the algorithms to their limits. Nonetheless, the plot demonstrates that the AR-DIC algorithm can assess the displacement despite the limited amplitude, providing qualitatively good results with similar performance for the different cases. On the other hand, the literature algorithms show a higher noise level in displacement estimation. All the algorithms show an overestimation of the displacement amplitude, which is reasonable taking into account that 1/100 pxl is generally considered the sensitivity limit for DIC algorithms. The computation was repeated for the same image set after adding random noise with an amplitude equal to 255/10, and the results are reported in Fig. 5(a) and (b), comparing the ground truth and the measured displacement in the case of 0.5 pxl and 0.01 amplitude respectively. Fig. 5(c) and (d) show the difference between the ground-truth displacement and the results of the different algorithms instead, for the case of 0.5 pxl and 0.01 amplitude respectively. Fig. 5(a) highlights that, for the case of 0.5 pxl amplitude, the added noise does not drastically impact the results, since the displacement amplitude is large. This is confirmed by Fig. 5(c), which shows only a slightly larger difference with respect to ground truth if compared with Fig. 4(c). For the case of 0.01 pxl amplitude, Fig. 5(b) shows that the AR-DIC algorithm (green, cyan and magenta lines) is still able to assess the displacement despite the relevant amount of noise in all cases 1–3. Literature algorithms show qualitatively worst measurement performances, with a higher noise level for both DICT (red line) and Ncorr (blue line).

These qualitative considerations were quantitively checked by computing SNR for all the studied elaborations as defined in Eq. (4), and the results are reported in Table 2.

Table 2 confirms that the AR-DIC algorithm always provides better results in comparison to other literature DIC methods. Looking at the SNR values for cases 1–3, it is possible to assess that all the considered three cases show similar performances, both in the theoretical simulation (no noise added to the data) and in the simulation with added noise. This suggests that using the resizing approach guarantees an improvement in measurement performance, while changing the other parameters (i.e. polynomial order and number of interpolating points) does not have a great impact on the measurement results. On the other hand, the literature algorithms show worse estimation performance regardless of the presence of noise in the image set. In particular, DICT always provides the worst results, especially in the case without added noise, while the Ncorr algorithm performs slightly better. Nevertheless, the SNR

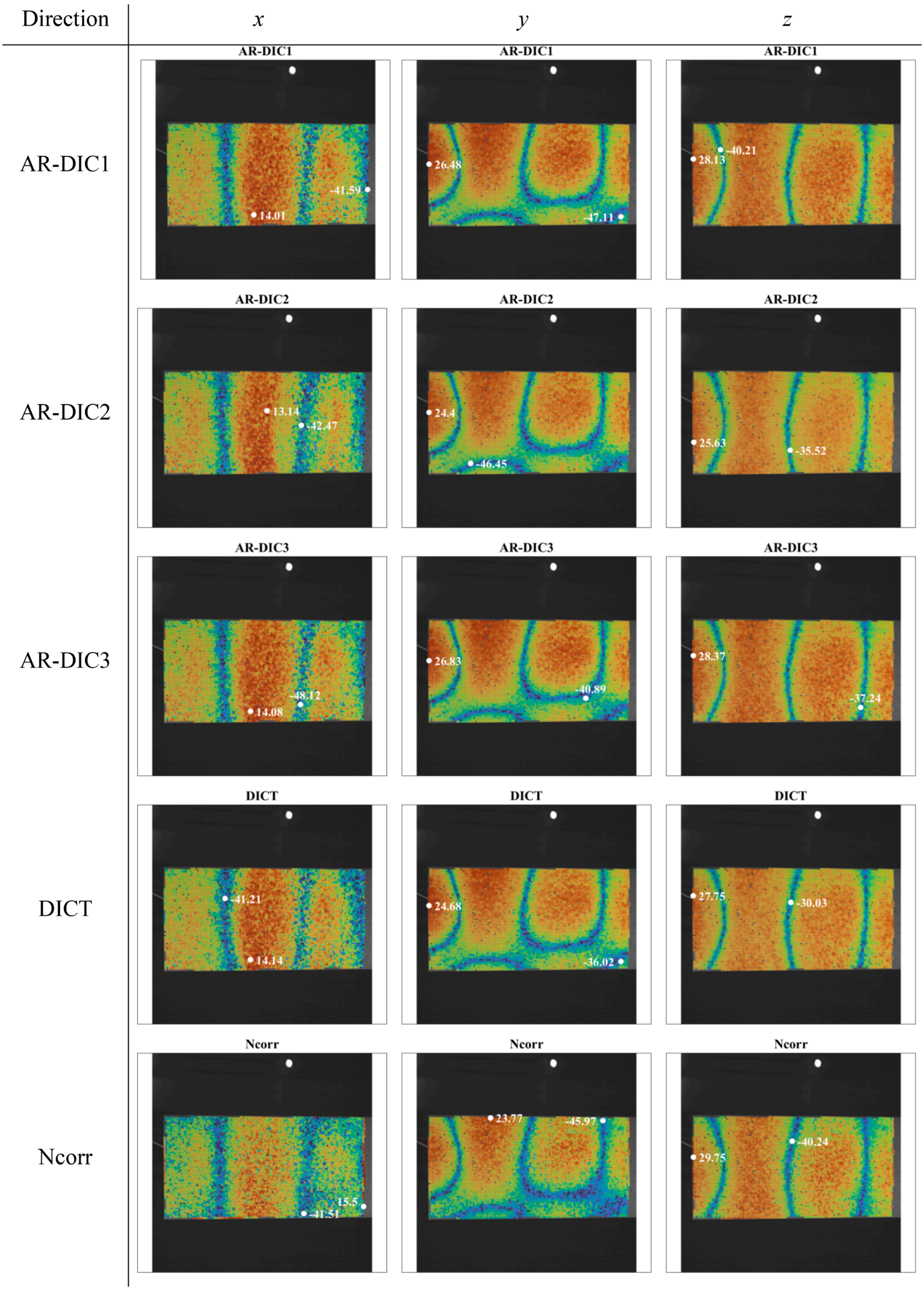

Fig. 8. SNR in the time domain for the considered algorithms along the three directions.

Table 3
Mean time domain SNR for different algorithms.

Algorithm	Mean T-SNR, Db		
	X	y	Z
AR-DIC1	−0.16	8.21	15.24
AR-DIC2	−1.26	7.77	13.73
AR-DIC3	−0.13	8.23	15.30
DICT	−0.95	7.60	14.15
Ncorr	−3.54	4.54	11.85

values obtained with the literature algorithms are always significantly lower with respect to the proposed AR-DIC algorithm, especially in the case of 0.01 pxl amplitude. The performances of the algorithms were also compared in terms of computational time, on a workstation equipped with an Intel Xeon W-3245 and 64.0 GB RAM. The results are reported in Table 2 for all the studied cases, averaging the timing needed to elaborate the images with noise and without noise and with the different amplitudes. As can be noted, the AR-DIC algorithms have the best performance, with an increasing computational time from cases 1 to 3. This is because cases 2 and 3 use the quartic polynomial function, which requires the Newton-Rapshon method to find the maximum correlation instead of a direct analytical solution (as for case 1). Additionally, case 3 uses a larger n_p, thus resulting in a longer computational time. On the other hand, DICT and Ncorr show longer times, even if the comparison is not straightforward since they are implemented in a Graphical User Interface and allow for a lower control on the processing, while the AR-DIC algorithms could be reduced to the essential operations.

To provide further insight into the effect of the different parameters on the AR-DIC results, the range $n_p = 1, \ldots 5$ and $r_f = 2, \ldots 5$ was investigated, both for the quadratic and quartic interpolation functions. The investigation was focused on the 0.01 pxl amplitude with added noise, i.e. the worst-case scenario. The results are reported in Fig. 6: the green curve is referred to the quadratic interpolation, while the red curve is referred to the quartic interpolation. As can be noted, the quartic interpolation performs slightly better than the quadratic interpolation for all the parameter values. Additionally, the plot highlights that increasing n_p is effective only in combination with increasing r_f. Moreover, further increasing the resizing factor above $r_f = 2$ does not provide significant advantages to the results.

4. Performance validation on experimental data

The considered algorithms were then tested on actual experimental data, measured on a cantilever plate vibrating under purely sinusoidal excitation. The right end of the plate (250 × 100 × 1.8 mm) was screwed to an electrodynamic shaker (TIRAvib TV51110). The shaker was controlled through an 8-channel LMS SCADAS Mobile in an open loop. A 3D DIC setup was used to perform the measurements since the cantilever plate's dominant motion is along the direction normal to its surface. The system was described and validated in [16], it is based on a pair of Optomotive TREX cameras and it exploits structured light scanning to solve the stereo matching problem. The displacement of corresponding points in left and right cameras image set was sequentially computed by using the discussed algorithms, i.e. AR-DIC, DICT and Ncorr. A subset size of 21 pxl was used to perform 2D DIC with all the algorithms, to have a fair comparison, on both left and right cameras image sets. The results of the camera pair were then triangulated to achieve 3D displacement maps, as deeply discussed in [16]. The experimental setup is shown in Fig. 7(a), along with the local coordinate system defined on the plate: the x axis is parallel to the longer plate's edge, while the z axis is perpendicular to the plate's surface. The deformed shape obtained at the frame corresponding to the vibration maximum at the selected excitation frequency is reported in Fig. 7(b-c), in terms of displacement along the x, y and z directions respectively. For brevity, only the results obtained with the AR-DIC1 algorithm were reported in the figure.

As can be noted, the main motion is found along the z direction, i.e. perpendicular to the plate surface, as expected. A relevant motion was measured also along the y direction, while a really small displacement was found along the x direction. The excitation frequency of 591 Hz was chosen to excite a mechanical resonance of the plate, to obtain a relevant displacement. Camera acquisition was set using a down-sampling approach [31] to acquire 50 frames during one vibration period. Two different criteria were used to compare the performance of different algorithms, by computing SNR both in time and spatial domain. It is worth noting that in experimental tests it is not possible to have a full-field ground-truth to compare the results with. Additionally, since purely sinusoidal excitation was performed (i.e. only one harmonic component is expected in the signal), frequency domain analysis was omitted since the computation of SNR already depicts the ratio between the relevant harmonic and the noise.

4.1. Time domain elaboration

Firstly, the same approach used for the synthetic data was repeated. Each measurement point on the image provides a signal in the time domain, and the displacement information is associated with the first harmonic (since one full period of the vibration was acquired). Thus, it was possible to compute the SNR associated with each measurement point, by comparing the contribution of the first harmonic with all the others. In this way, an SNR map can be drawn on the image, showing the quality of the measurement in each location. Each DIC algorithm provides a different time domain SNR map to be compared. The results obtained for the three directions are reported in Fig. 8, with the same color scale for all the algorithms and each direction. The maps clearly show that, for each algorithm, the SNR has a minimum in correspondence to the nodal lines of the structure, since the displacement is zero and the measurement is dominated by noise. On the other hand, higher SNRs can be noted in correspondence with the displacement maxima, as expected. Minimum and maximum SNR values were added in Fig. 8 for reference. The analysis of Fig. 8 highlights that, again, the AR-DIC algorithm provides really similar results for all three cases, with the highest SNR values close to the maxima of the deformed shape. In this analysis, also the DICT algorithm shows a good performance, which is qualitatively comparable to the AR-DIC algorithm. On the other hand, Ncorr provides the worst performances, since the SNR values are generally lower in the whole measurement field.

The information of the full map can be condensed into a single scalar, which can be obtained by computing the mean value of the SNR through the measurement points (Mean T-SNR). The results are reported in Table. 3. As can be noted, the column corresponding to the x direction presents negative values, because the displacement amplitude is the lowest among the three directions. The y and z directions instead present positive SNR values, corresponding to the larger displacement amplitudes. The results confirm that the AR-DIC algorithm (cases 1–3) and DICT have comparable results, while Ncorr provides a lower mean SNR value for all the analyzed directions.

4.2. Spatial domain elaboration

The algorithms' performance was also evaluated in the spatial domain. Indeed, the accuracy and robustness of the algorithms can be assessed for a single image, by evaluating the smoothness of the displacement map along the plate surface, since adjacent measurement points should have similar displacement values. This can be done by rearranging the displacement map in a 1-D array and scoping all the measurement points from left to right and from top to bottom. An example of the result, for the frame corresponding to the maximum displacement measured over time, is reported in Fig. 9(a) for the three directions: the horizontal axis of the plot reports the considered point number, while the vertical axis shows the corresponding displacement value. The blue line is referred to the results of the Ncorr algorithm, while the green line is referred to the AR-DIC algorithm (only case 1 was reported, for readability). As can be noted, the displacement across the measurement points is characterized by some low spatial-frequency contributions, which represent the actual smooth deformed shape, and high spatial-frequency contributions, which represent measurement noise. The black line was added to the plots as a reference, and was obtained by applying a moving average filter to the results of the AR-DIC1 algorithm. A visual comparison between the blue and the green line confirms that the AR-DIC algorithm achieves a lower noise level with respect to Ncorr, which shows several high-intensity spikes in the data, denoting a higher noise level in the spatial domain. This is particularly visible for the x direction, which is characterized by lower amplitudes. A quantitative comparison of the results can be obtained by computing the spatial domain SNR of the data in Fig. 9(a), and repeating the computation for all the acquired frames. The results obtained for the different algorithms are reported in Fig. 9(b), where green, cyan, magenta, red and blue lines refer to Case 1, Case 2, Case 3, DICT and Ncorr, respectively. The three directions were condensed in the same plot, and a label denote the data corresponding to the x, y and z directions (from lower to higher, respectively).

All the plots have a similar trend over the frames, ranging from low

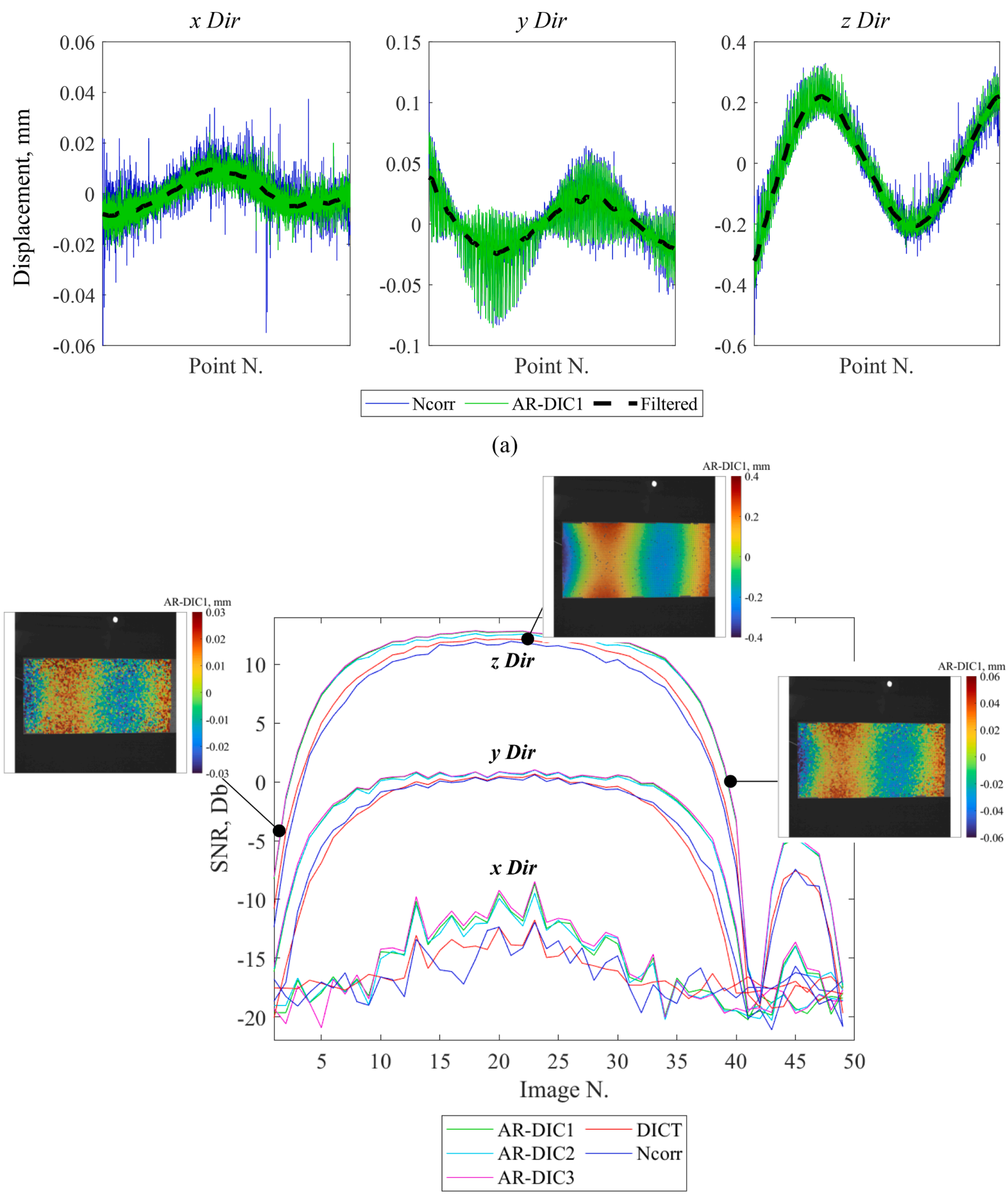

Fig. 9. Spatial domain comparison: (a) displacement across measurement points along the three directions and (b) spatial SNR along the time series for the three directions.

Table 4
Mean spatial domain SNR for different algorithms.

Algorithm	Mean S-SNR, Db		
	x	y	z
AR-DIC1	−15.70	−4.68	5.77
AR-DIC2	−15.84	−4.66	5.66
AR-DIC3	−15.62	−4.53	5.87
DICT	−17.55	−6.24	4.17
Ncorr	−17.91	−6.13	3.60

to high SNR values depending on the displacement amplitude of each frame. In particular, higher displacements (such as frames 15–30) provide higher and positive SNRs, since the signal is clearly visible in comparison to the noise. On the other hand, lower displacements (such as frames 35–40) provide lower SNRs in the negative region, meaning that the noise intensity is higher than the signal. To qualitatively assess the appearance of the displacement maps corresponding to different SNR values, the maps along z direction for three different frames were overlapped on the plot: frame 22 (SNR: 12.84 Db), frame 39 (SNR: −3.17 Db) and frame 3 (SNR: −5.70 Db), elaborated with AR-DIC1. Clearly, a high positive SNR corresponds to a smooth map in the spatial domain, such as frame 22. Nevertheless, even a low and negative SNR value provides relevant information: as can be noted by frame 39, the same spatial trend of frame 22 can be observed, despite the much lower amplitude. Additionally, even if frame 3 has a low SNR, a similar spatial trend can be noted, even if dominated by noise. The plot confirms that AR-DIC algorithms outperform the literature algorithms, providing higher spatial SNR values for all the frames. Again, cases 1–3 have really similar performances, with case 2 showing a slightly lower data quality. This confirms that the main advantage is achieved by applying the resizing scheme, while acting on the correlation interpolation has a negligible impact on the results. On the other hand, DICT and Ncorr show comparable results, with a maximum spatial SNR value of about 11.95 Db, substantially lower than AR-DIC algorithms that show a maximum spatial SNR value of approximately 12.84 Db for the z direction. Similar considerations can be drawn for the y direction, where DICT and Ncorr show a maximum SNR value of 0.61 Db while AR-DIC reaches 1.03 Db. For both z and y directions, the discrepancies between different algorithms are more evident in the low SNR regions, where higher subpixel accuracy is needed. The plot corresponding to the x direction emphasizes this discrepancy since AR-DIC reaches an SNR of −8.49 Db while the maximum SNR value for Ncorr and DICT is −12.98 Db. This lower amplitude direction further highlights the effectiveness of the proposed AR-DIC algorithm in measuring small amplitude displacements, which represent the hardest challenges in full-field vibration measurements. Finally, the quantitative performance of the algorithms along different directions can be assessed by computing the man value of SNR along the frameset (similarly to the results of Table. 3). The so-defined spatial mean SNR (Mean S-SNR) is reported in Table. 4 for all the studied algorithms and displacement directions. The table highlights that the proposed AR-DIC algorithm (for all cases 1–3) always provides better performances with respect to the literature methods, which instead have comparable and lower outcomes.

5. Conclusions

The paper presents a method to perform Digital Image Correlation by enhancing the sub-pixel accuracy, which is of utmost importance for small displacement measurements such as mechanical vibrations. Two different approaches were investigated: enhancing the image resolution and improving the polynomial interpolation. The image resolution can be leveraged by using resizing algorithms, which allow interpolating pixel information and obtaining smoother grayscale levels across the subsets. The polynomial interpolation can be improved by changing the polynomial order and increasing the number of points used for the interpolation. Both strategies were implemented in the Augmented Resolution Digital Image Correlation (AR-DIC) algorithm, newly introduced in this paper. By changing the algorithm parameters, different scenarios were tested: resized subset with quadratic polynomial across one interpolation point, resized subset with quartic polynomial across one interpolation point and resized subset with quartic polynomial across two interpolation points. These three variants of the AR-DIC algorithm were tested on both synthetic and experimental data, and compared with the performance of literature approaches, in particular the DICT and the Ncorr algorithms. The performed campaign allowed to assess that the AR-DIC algorithm can measure small-amplitude displacements, even in the presence of relevant noise, and it outperforms the literature approaches in all the testing scenarios in terms of SNR. Among the different tested configurations, it was noted that augmenting the resolution provides most of the advantage, while changing the polynomial order and the number of interpolation points has a lower impact on the final results. Further developments could be focused on the study of different non-polynomial functions for correlation map interpolation (e.g. splines). Additionally, FFT-based methods for correlation computation represent a promising alternative to the convolution approaches in the spatial domain (i.e. Eq. (1) and could drastically reduce the computational time for large image datasets, thus their use in combination with the proposed augmented resolution approach could be investigated. Finally, the impact of the AR-DIC algorithm as a first guess for a global DIC method could be investigated, trying to further push DIC sensitivity to the smallest displacement limit.

CRediT authorship contribution statement

Paolo Neri: Writing – review & editing, Writing – original draft, Validation, Software, Methodology, Investigation, Formal analysis, Conceptualization.

Declaration of competing interest

The authors declare that they have no known competing financial interests or personal relationships that could have appeared to influence the work reported in this paper.

Data availability

Data will be made available on request.

References

[1] L. Bertini, P. Neri, C. Santus, A. Guglielmo, Automated Experimental modal analysis of bladed wheels with an anthropomorphic Robotic Station, Exp Mech 57 (2017), https://doi.org/10.1007/s11340-016-0223-5.
[2] A. Rodriguez, J.L. Kauffman, Characterization of Blisk Mistuning Induced by Bonded Piezoelectric Elements, in: AIAA Science and Technology Forum and Exposition, AIAA SciTech Forum 2022, 2022. 10.2514/6.2022-1691.
[3] R. Wu, D.S. Zhang, Q.F. Yu, Y.X. Jiang, D. Arola, Health monitoring of wind turbine blades in operation using three-dimensional digital image correlation, Mech Syst Signal Process 130 (2019) 470–483, https://doi.org/10.1016/j.ymssp.2019.05.031.
[4] A. Kamariotis, E. Chatzi, D. Straub, A framework for quantifying the value of vibration-based structural health monitoring, Mech Syst Signal Process 184 (2023), https://doi.org/10.1016/j.ymssp.2022.109708.
[5] T.C. Chu, W.F. Ranson, M.A. Sutton, Applications of digital-image-correlation techniques to experimental mechanics, Exp Mech 25 (1985), https://doi.org/10.1007/BF02325092.
[6] F. Hild, S. Roux, Digital image correlation: from displacement measurement to identification of elastic properties - a review, Strain 42 (2006), https://doi.org/10.1111/j.1475-1305.2006.00258.x.
[7] J.R. Warburton, G. Lu, T.M. Buss, H. Docx, M.Y. Matveev, I.A. Jones, Digital image Correlation vibrometry with low speed equipment, Exp Mech 56 (2016) 1219–1230, https://doi.org/10.1007/s11340-016-0162-1.
[8] E. Di Lorenzo, D. Mastrodicasa, L. Wittevrongel, P. Lava, B. Peeters, Full-field modal analysis by using digital image correlation technique, in: In: Conference Proceedings of the Society for Experimental Mechanics Series, 2020, https://doi.org/10.1007/978-3-030-47721-9_15.

[9] M.N. Helfrick, C. Niezrecki, P. Avitabile, T. Schmidt, 3D digital image correlation methods for full-field vibration measurement, Mech Syst Signal Process 25 (2011) 917–927, https://doi.org/10.1016/j.ymssp.2010.08.013.
[10] P. Song, A. Trivedi, C.R. Siviour, Tensile testing of polymers: integration of digital image correlation, infrared thermography and finite element modelling, J Mech Phys Solids 171 (2023), https://doi.org/10.1016/j.jmps.2022.105161.
[11] S.B. Lindström, H. Wemming, Z. Kapidžić, M.S. Loukil, M. Segersäll, Integrated digital image correlation for mechanical characterization of carbon fiber-reinforced polymer plates, Compos Struct 305 (2023), https://doi.org/10.1016/j.compstruct.2022.116501.
[12] Y. Blikharskyy, N. Kopiika, R. Khmil, J. Selejdak, Z. Blikharskyy, Review of development and application of digital image Correlation method for study of stress-strain state of RC structures, Appl. Sci. (switzerland) 12 (2022), https://doi.org/10.3390/app121910157.
[13] J. Javh, J. Slavič, M. Boltežar, High frequency modal identification on noisy high-speed camera data, Mech Syst Signal Process 98 (2018), https://doi.org/10.1016/j.ymssp.2017.05.008.
[14] T.J. Beberniss, D.A. Ehrhardt, High-speed 3D digital image correlation vibration measurement: recent advancements and noted limitations, Mech Syst Signal Process 86 (2017) 35–48, https://doi.org/10.1016/j.ymssp.2016.04.014.
[15] Y. Kato, S. Watahiki, Vibration mode identification method for structures using image correlation and compressed sensing, Mech Syst Signal Process 199 (2023), https://doi.org/10.1016/j.ymssp.2023.110495.
[16] P. Neri, Frequency-band down-sampled stereo-DIC: beyond the limitation of single frequency excitation, Mech Syst Signal Process 172 (2022), https://doi.org/10.1016/j.ymssp.2022.108980.
[17] L. Ruixin, Z. Sheng, B. Chen, Z. Gao, Y. Fu, Modal shapes measurements of a rotating disc using stroboscopic 3D digital image correlation and down-sampling strategy, in: 2023. 10.1117/12.2667027.
[18] J. Blaber, B. Adair, A. Antoniou, Ncorr: open-source 2D digital image Correlation matlab Software, Exp Mech 55 (2015), https://doi.org/10.1007/s11340-015-0009-1.
[19] C. Eberl, Digital Image Correlation and Tracking (2010). https://it.mathworks.com/matlabcentral/fileexchange/12413-digital-image-correlation-and-tracking.
[20] G. Besnard, H. Leclerc, F. Hild, S. Roux, N. Swiergiel, Analysis of image series through global digital image correlation, J. Strain Anal. Eng. Des. 47 (2012), https://doi.org/10.1177/0309324712441435.
[21] B. Pan, B. Wang, G. Lubineau, A. Moussawi, Comparison of subset-based local and finite element-based global digital image Correlation, Exp Mech 55 (2015), https://doi.org/10.1007/s11340-015-9989-0.
[22] J. Yang, K. Bhattacharya, Augmented lagrangian digital image Correlation, Exp Mech 59 (2019), https://doi.org/10.1007/s11340-018-00457-0.
[23] J. Yang, L. Hazlett, A.K. Landauer, C. Franck, Augmented lagrangian digital volume Correlation (ALDVC), Exp Mech 60 (2020), https://doi.org/10.1007/s11340-020-00607-3.
[24] J. Yang, K. Bhattacharya, Fast adaptive mesh augmented lagrangian digital image Correlation, Exp Mech 61 (2021), https://doi.org/10.1007/s11340-021-00695-9.
[25] P.-C. Hung, A.S. Voloshin, In-plane strain measurement by digital image correlation, J. Braz. Soc. Mech. Sci. Eng. 25 (2003) 215–221.
[26] B. Pan, H.M. Xie, B.Q. Xu, F.L. Dai, Performance of sub-pixel registration algorithms in digital image correlation, Meas Sci Technol (2006), https://doi.org/10.1088/0957-0233/17/6/045.
[27] L. Pallotta, G. Giunta, C. Clemente, Subpixel SAR image registration through Parabolic interpolation of the 2-D cross Correlation, IEEE Trans. Geosc. Remote Sens. 58 (2020), https://doi.org/10.1109/TGRS.2019.2961245.
[28] M.B. Tomás, B. Ferrer, D. Mas, Influence of neighborhood size and cross-correlation peak-fitting method on location accuracy, Sensors (switzerland) 20 (2020), https://doi.org/10.3390/s20226596.
[29] G. Peters, WILKINSON JH, /least squares problem and pseudo- inverses, Computer Journal 13 (1970), https://doi.org/10.1093/comjnl/13.3.309.
[30] T.J. Ypma, Historical development of the Newton-raphson method, SIAM Review 37 (1995), https://doi.org/10.1137/1037125.
[31] P. Neri, A. Paoli, A.V. Razionale, C. Santus, Time-domain image filtering for DIC vibration measurements, J Phys Conf Ser (2021), https://doi.org/10.1088/1742-6596/2041/1/012008.